Journal of Membrane Science 487 (2015) 162–172

Contents lists available at ScienceDirect

Journal of Membrane Science

journal homepage: www.elsevier.com/locate/memsci

Fabricating graphene oxide-based ultrathin hybrid membrane for pervaporation dehydration via layer-by-layer self-assembly driven by multiple interactions

Jing Zhao [a,b], Yiwei Zhu [a,b], Fusheng Pan [a,b], Guangwei He [a,b], Chenhao Fang [a,b], Keteng Cao [a,b], Ruisi Xing [a,b], Zhongyi Jiang [a,b,*]

[a] Key Laboratory for Green Chemical Technology of Ministry of Education, School of Chemical Engineering and Technology, Tianjin University, Tianjin 300072, China

[b] Collaborative Innovation Center of Chemical Science and Engineering (Tianjin), Tianjin 300072, China

ARTICLE INFO

Article history:
Received 14 January 2015
Received in revised form
26 March 2015
Accepted 29 March 2015
Available online 4 April 2015

Keywords:
Gelatin/graphene oxide
Layer-by-layer self-assembly
Multiple interactions
Ultrathin hybrid membrane
Pervaporation dehydration

ABSTRACT

Graphene oxide (GO)-based ultrathin hybrid membranes with thicknesses less than 115 nm were fabricated via layer-by-layer (LbL) self-assembly driven by multiple interactions. Gelatin (GE) and GO were alternately deposited on hydrolyzed polyacrylonitrile (H-PAN) ultrafiltration membranes through electrostatic attraction, hydrogen bond, and hydrophobic interaction to obtain hybrid multilayer membranes. The incorporation of GO favored the coverage of nanopores on H-PAN membrane, which greatly reduced the required deposition cycles for acceptable permselectivity of membrane, and then simplified the membrane-fabrication procedure. Enhanced thermal stability of GE molecules was obtained for as-fabricated hybrid multilayer membranes compared with GE/H-PAN pristine membrane. In membrane separation experiments, the hybrid multilayer membrane achieved synchronous enhancement in permeation flux and separation factor for pervaporation dehydration of ethanol aqueous solution in comparison with GE/H-PAN pristine membrane. The pH value of 4.0 was determined as the optimal condition of self-assembly process in terms of separation performance. The optimized separation performance of hybrid multilayer membranes with the bilayer number 10.5 was obtained with the permeation flux of 2275 g/m^2 h and water content in permeate of 98.7 wt% under the conditions of 350 K and water content in feed of 20 wt%. Desirable operation stability was acquired in the long-term membrane separation experiment.

1. Introduction

Fabricating composite membrane with ultrathin, defect-free and stable active layer has been a research focus in membrane field due to its great potential in achieving high permeability, selectivity and stability synchronously [1]. In this regard, the seashell nacre provides rich inspirations for the preparation of membrane with ultrahigh mechanical stability: the ordered "brick-and-mortar" arrangement of organic and inorganic layers, strong interfacial interaction, and high interfacial compatibility enable efficient loading transfer between organic and inorganic phases; the resultant synergistic effect between two phases endows the hybrid nacre with outstanding mechanical properties [2–4]. Compared with other methods for preparing layered organic-inorganic hybrid membrane (such as vacuum filtration [5] and coupling precipitation reactions with self-organizing surfactants [6]), layer-by-layer (LbL) self-assembly displays distinct merits such as stronger and more controllable interfacial interactions, higher degree of structure control and better nanoscale organization [3,5,7]. To imitate the microstructure of nacre and acquire high performance, two-dimensional inorganic materials should be the preferential candidates as the building blocks of LbL self-assembly. Graphene oxide (GO) is particularly an ideal choice because of its atomic thickness, high specific surface area, outstanding mechanical strength, and tunable physicochemical properties [8–10]. Moreover, GO bears abundant hydrophilic groups [11], imparting great potential for broad application in water-permeating membranes [12,13]. Therefore, fabricating layered polymer/GO hybrid membrane via LbL self-assembly seems a promising strategy to obtain ultrathin, defect-free and stable active layer.

For the structural optimization of hybrid membrane, a precisely engineered organic-inorganic interface is critical. The molecular and nanoscale engineering of interfaces relies heavily on manipulation of interfacial interactions [5,14,15]. Electrostatic attraction

* Corresponding author at: Key Laboratory for Green Chemical Technology of Ministry of Education, School of Chemical Engineering and Technology, Tianjin University, Tianjin 300072, China. Tel./fax: +86 22 23500086.
E-mail address: zhyjiang@tju.edu.cn (Z. Jiang).

http://dx.doi.org/10.1016/j.memsci.2015.03.073
0376-7388/

was the main interaction between GO and polymers in the reported studies of fabricating polymer/GO hybrid separation membranes via LbL self-assembly. Grunlan et al. [16] and Mi et al. [17] fabricated polyethylenimine (PEI)/GO and poly(allylamine hydrochloride) (PAH)/GO multilayer membranes for gas separation and forward osmosis, respectively. Zhang et al. employed sequential assembly of PEI-modified GO and polyacrylic acid to fabricate multilayer membrane for pervaporation and nanofiltration [18]. The formation of electrostatic attraction arises from the negatively charged carboxyl groups on GO, which merely exist at the edge of GO with low content. Therefore, the interaction sites between GO and polymers in these cases are quite limited.

GO possesses amphiphilic structure with hydrophobic carbon backbone and hydrophilic polar groups on their basal plane and edges. Manipulating the multiple interactions between GO and the pairing polymer, thus making the utmost use of the various groups on GO will be a facile approach to increase interaction sites between adjacent layers and create more stable interfaces [8]. Gelatin (GE) is a natural protein with both hydrophilic and hydrophobic amino acid side chains [19]. As a polyampholyte, GE is positively charged under acidic condition arising from protonated amino groups [19]. Consequently, multiple interactions including electrostatic attraction, hydrogen bond and hydrophobic interaction can be formed between GE and GO. In addition, GE is a suitable membrane material utilized in water-related separation processes due to its high hydrophilicity and excellent film-forming ability [19,20].

In this study, GE and GO were utilized to fabricate ultrathin hybrid membrane on hydrolyzed polyacrylonitrile (H-PAN) ultrafiltration membrane via LbL self-assembly driven by multiple interactions. The hydrophilicity, physical morphology, chemical structure, and thermal property of hybrid multilayer membranes were extensively characterized. Using pervaporation dehydration of ethanol aqueous solution as a model system, the effect of bilayer number, pH value, operation temperature and water content in feed on separation performance was investigated. The long-term operation stability of hybrid multilayer membrane was also assessed.

2. Experimental

2.1. Materials

Gelatin from porcine skin (Type A, Bloom 300) was supplied by Sigma-Aldrich (USA). Natural flake graphite (2500 mesh) was purchased from Qingdao Tianhe Graphite Co. Ltd. (Shandong, China). The flat-sheet polyacrylonitrile (PAN) ultrafiltration membrane with a molecular weight cut-off of 100 000 was received from Shandong MegaVision Membrane Technology & Engineering Co. Ltd. (Shandong, China). Hydrochloric acid (HCl, 36–38 wt%), sulfuric acid (H_2SO_4, 98 wt%) and potassium permanganate ($KMnO_4$) were purchased from Tianjin Kewei Ltd. (Tianjin, China). Hydrogen peroxide aqueous solution (H_2O_2, 30 wt%), sodium nitrate ($NaNO_3$), ethanol ($\geq$99.7 wt%) and sodium hydroxide (NaOH) were received from Tianjin Guangfu Fine Chemical Research Institute (Tianjin, China). All the reagents were of analytical grade and used as received. Deionized water was used throughout the experiments.

2.2. Membrane fabrication

2.2.1. Preparation of GO

GO dispersion was prepared following the modified Hummers method [21]. 115 mL of 98 wt% H_2SO_4 was added into a flask in ice bath. After the temperature was lower than 5 °C, 5 g of graphite powder and 2.5 g of $NaNO_3$ were added under stirring. Then 15 g of $KMnO_4$ was added slowly in batches to keep the temperature under 5 °C. After stirring for 2 h, the flask was transferred into an oil bath at 35 ± 2 °C. 30 min later, 230 mL of water was added dropwise with the temperature of mixture below 100 °C (a large amount of heat would be liberated during this process). Then the temperature of oil bath was set at 98 °C and kept for 3 h. Afterwards, the viscous mixture was poured into a beaker and diluted with 1 L of deionized water, followed by adding 30 mL of H_2O_2. Finally, the mixture was centrifuged and washed with HCl solution for three times, and then washed with water until the pH of supernatant was about 7.0. The yellow-brown GO dispersion could be obtained by dispersing the centrifuged sediment in deionized water and sonicating the resultant aqueous solution.

2.2.2. Fabrication of hybrid multilayer membranes

The hybrid multilayer membranes were fabricated via LbL self-assembly employing a home-made single-side dip-coating device to avoid the deposition of GE and GO on the nonwoven fabric side of ultrafiltration membrane [19]. 2 mg/ml GE solution was prepared by dissolving GE in deionized water at 60 °C and stirring for 1 h. GO was dispersed in deionized water with a concentration of 0.4 mg/ml, and sonicated for 30 min. After sonication, a 10 min centrifugation at 3000 rpm was used to remove the thick multilayer flakes (sediment) and collect the exfoliated graphene oxide (supernatant). The pH values of GE solution and GO dispersion were adjusted to 4.0 utilizing 0.1 mol/L HCl and NaOH solutions, respectively. Prior to the deposition of GE and GO, the PAN ultrafiltration membranes were hydrolyzed by being soaked in 1.5 mol/L NaOH aqueous solution at 55 °C for 30 min, and then rinsed with deionized water until the pH value reached about 7.0. Subsequently, the H-PAN membrane was mounted in the single-side dip-coating device with the H-PAN surface side up and the nonwoven fabric side down. The LbL self-assembly process was shown in Fig. S1. GE solution and GO dispersion were alternately poured into the device and kept still for 5 min. After each deposition, the membrane was rinsed with deionized water for three times. Finally, the membrane was taken out and dried at room temperature after pre-determined times of deposition and rinse. It should be pointed out all the membranes possessed a GE innermost layer and a GE outermost layer. The resultant membranes were designated as $(GE/GO)_X$/H-PAN, where X represented the bilayer number of GE/GO (from 2.5 to 10.5). For comparison, GE/H-PAN pristine membrane was prepared by pouring 8 mg/ml of GE solution into the same device utilized in LbL self-assembly process. After kept still for 5 min, the membrane was taken out and dried at room temperature. In addition, control experiments were conducted by fabricating hybrid multilayer membranes with a constant bilayer number of 10.5 under pH value of 2.0 and 6.0.

2.3. Membrane characterization

The morphology of GO was observed by transmission electron microscopy (TEM, JEOL JEM-100CXII) and atomic force microscope (AFM, CSPM 5000), respectively. Wide-angle X-ray diffraction (XRD) patterns were used to investigate the crystallization properties of GO by a D/MAX-2500 X-ray diffractometer (CuKα). FTIR spectra in the range of 4000–500 cm^{-1} were recorded on a BRUKER Vertex 70 FT-IR spectrometer equipped with a horizontal attenuated transmission accessory for GO and a horizontal attenuated total reflectance accessory for the membranes. Raman spectrum of GO was obtained by a DXR Smart Raman Spectrometer (Thermo Fisher Scientific). The chemical compositions of GO and hydrolyzed PAN were measured by X-ray photoelectron spectroscopy (XPS, Kratos Axis Ultra DLD) with a monochromatic Al Kα source and a charge neutralizer. The surface charge property of GO was characterized in their aqueous dispersion by a Malvern

Nano ZS zeta-potential analyzer. The morphology of membrane surface was observed by field emission scanning electron microscope (FESEM) (Nanosem 430). The cross-section image of membrane was also obtained by FESEM to observe the morphology and measure the thickness of the active layer. The surface hydrophilicity of membrane was evaluated by measuring the static water contact angle at room temperature by a contact angle goniometer (JC2000C Contact Angle Meter). Each membrane should be measured at least six times at different locations of the surface and average data was taken as the final result. To acquire the thermal properties of GE and GE/GO complex, thermogravimetric analysis (TGA, NETZSCH TG 209 F3) was used over the range of 40–800 °C with a heating rate of 10 °C min^{-1} under nitrogen flow.

2.4. Pervaporation experiment

Pervaporation is an important membrane process for the separation of liquid mixture, especially for removal of water from organic solvent. In this study, the separation performance of as-fabricated membranes was evaluated utilizing the pervaporation dehydration of ethanol aqueous solution as a model system.

Pervaporation experiments were performed on the P-28 membrane module (CM-Celfa AG Company, Switzerland) with an effective membrane area of 25.6 cm^2. The down-stream pressure was kept below 0.3 kPa using a vacuum pump, and the flow rate of feed solution was controlled at 60 L/h. For each pervaporation experiment, the 1 h stable time was ensured before the permeate was collected with a cold trap immersed in liquid nitrogen. The mass of permeate solutions collected at an interval of 0.5 h were weighted. The compositions of feed and permeate solutions were determined by gas chromatography (Agilent4890, USA). The separation performance of membrane was evaluated by permeation flux (J, g/(m^2 h)), separation factor (α) and pervaporation separation index (PSI) calculated via the following equations:

$$J = \frac{Q}{A \times t} \tag{1}$$

$$\alpha = \frac{P_W/P_E}{F_W/F_E} \tag{2}$$

$$PSI = J \times (\alpha - 1) \tag{3}$$

where Q is the mass of permeate (g) collected during a time interval of t (h), A is the effective membrane area in contact with the feed (m^2). P and F represent the mass fractions of water (with the subscript W) or ethanol (with the subscript E) in the permeate and feed solutions, respectively.

In addition, the permeance of individual components ($(P/l)_i$, GPU) (1 GPU = 7.501×10^{-12} m^3 (STP)/m^2 s Pa) and selectivity (β) were calculated by the following equations:

$$(P/l)_i = \frac{J_i}{p_{i0} - p_{il}} = \frac{J_i}{\gamma_{i0} x_{i0} p_{i0}^{sat} - p_{il}} \tag{4}$$

$$\beta = \frac{(P/l)_W}{(P/l)_E} \tag{5}$$

where J_i is the permeation flux of component i (g/(m^2 h)), l is the thickness of membrane (m), p_{i0}, p_{il} are the partial pressures of component i in the feed side and permeate side (Pa), p_{il} can be calculated approximately as 0 for the high vacuum degree in the permeate side. γ_{i0} and x_{i0} are the activity coefficient and mole fraction of component i in the feed liquid, respectively. p_{i0}^{sat} is the saturated vapor pressure of pure component i at operation temperature (Pa). The permeation flux of water and ethanol should be transformed into the volumes under standard temperature and pressure (STP): 1 kg of water vapor at STP = 1.245 m^3 (STP), 1 kg of ethanol vapor at STP = 0.487 m^3 (STP) [29]. To guarantee the reliability of experimental data, three duplicated samples were fabricated under the same condition, and the pervaporation experiments for each sample were repeated for three times. The measurement results of three samples were averaged as the final data with deviations shown in figures as error bars.

3. Results and discussion

3.1. Characterization of GO

The chemical and physical structures of GO were characterized as shown in Fig. 1. The typical lamellar morphology of GO with a myriad of wrinkles and high transparency is observed in Fig. 1a. The AFM image in Fig. 1b shows that the GO sheets possess irregular shape and micrometer-scale size along horizontal direction. The thickness of GO sheets is measured to be about 0.65 nm from the height profile in inset, indicating the high-extent exfoliation. The FT-IR spectra of graphite and GO were obtained to confirm the oxidation reaction of graphite (Fig. 1c). Compared with the spectrum of graphite, many new characteristic peaks are observed on that of GO. The peaks at 3400 cm^{-1}, 1734 cm^{-1}, 1620 cm^{-1}, and 1083 cm^{-1} are attributed to the stretching vibration of hydroxyl, stretching vibration of carbonyl in carboxyl, asymmetrical stretching vibration of carboxylate, and stretching vibration of epoxy group, respectively. Consequently, it can be concluded that hydroxyl, carboxyl, and epoxy groups are generated through oxidation reaction. Fig. S2a exhibits the XRD patterns for graphite and GO. The sharp diffraction peak at $2\theta = 26.6°$ (crystallographic plane 002) on XRD pattern for graphite corresponds to a d-spacing of 0.336 nm. By contrast, GO shows a broader and weaker peak at $2\theta = 12.2°$ (crystallographic plane 001, corresponding to a d-spacing of 0.733 nm). The variation of peak shape and position can be ascribed to the increase of structural disorder and the formation of oxygen-containing groups after oxidation reaction, respectively [22]. The Raman spectrum of GO (Fig. S2b) shows a G band at 1590 cm^{-1} assigning to the sp^2 hybridized carbon atoms, and a D band at 1350 cm^{-1} belonging to local defects and disorder, which confirms the formation of structural defects on GO after oxidization reaction. XPS results were analyzed to obtain the chemical composition of GO. The low C/O ratio of 2.0 (Fig. 1d) indicates a high oxidation degree [13,22,23]. The C1s core level spectrum of GO (Fig. 1e) shows three peaks at binding energies of 284.5 eV, 286.5 eV, and 287.7 eV, which are attributed to C–C/C=C (55.96%), C–O/O–C–O (27.31%) and O–C=O (16.73%), respectively [24,25].

The zeta potential of GO at different pH values was measured as shown in Fig. 2a to determine the suitable pH of GE solution and GO dispersion for the self-assembly process. Due to the promoted ionization of COOH to COO^- at higher pH, the zeta potential of GO decreases from −20.9 to −45.8 mV with pH varying from 2.0 to 7.0. Afterwards, the zeta potential exhibits a growing tendency with pH value, resulting from the compression of double electric layer outside GO at higher ionic concentration [22]. To achieve a self-assembly process with high interlayer cross-linking density, both GE and GO need to be adsorbed in a highly charged state [26]. GE is a polyampholyte with a isoelectric point of 8–9 [20], which means GE is positively charged in acid solution, and more positive charges are generated at lower pH. Due to the reverse variation trend of the charge amount on GE and GO with pH, a moderate pH should be chosen to maximize the cross-linking density. It can be observed from Fig. 2a that the decrease of zeta potential in the pH range of 4.0–7.0 is not so remarkable as that in the pH range of 2.0–4.0, indicating that fewer negative charges will be generated on GO with pH increasing from 4.0 to 7.0 while sacrificing positive charges on GE. Therefore, the pH values of GE solution and GO dispersion were determined as 4.0. Fig. 2b exhibits the images of

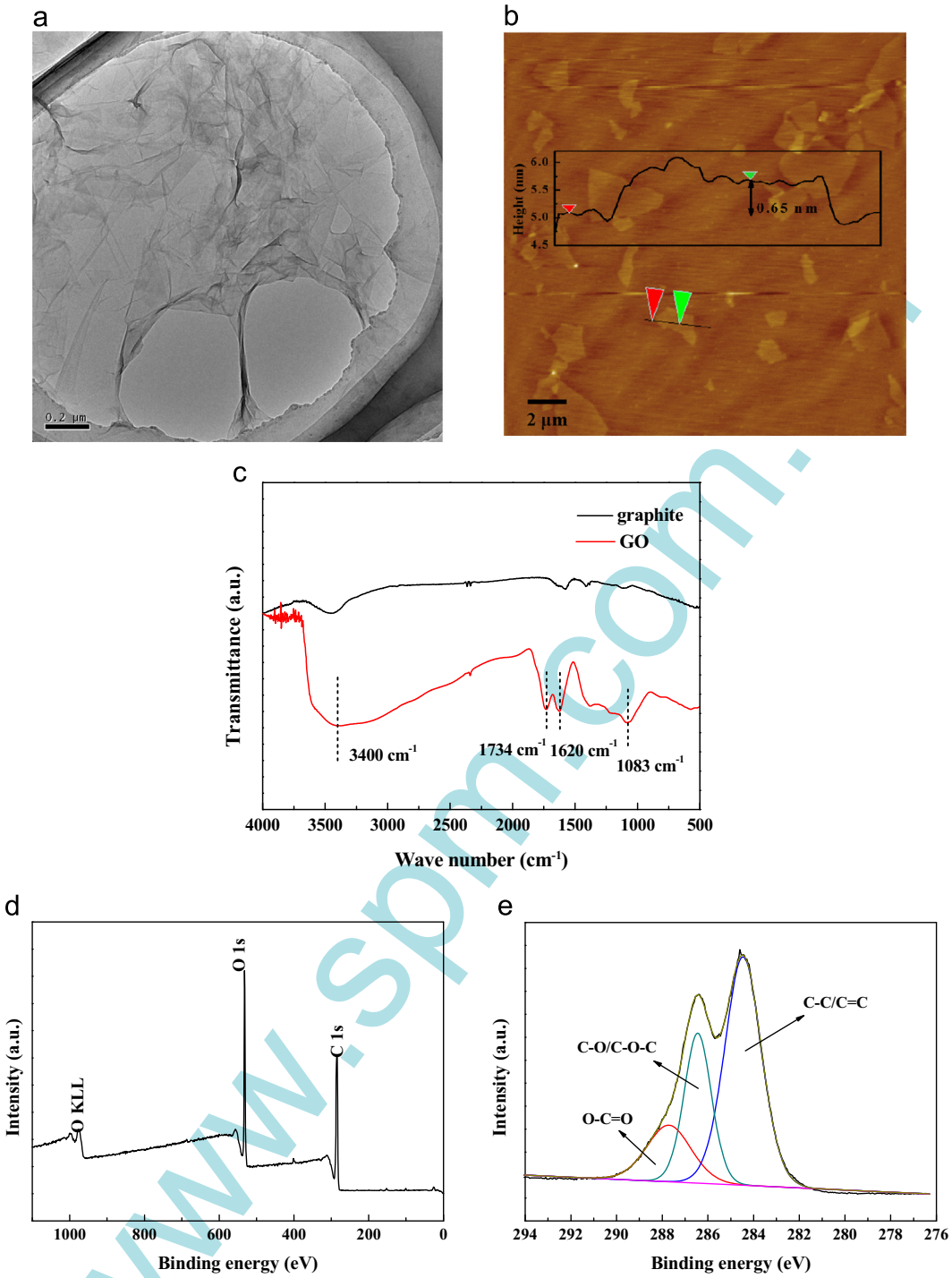

Fig. 1. (a) TEM image of GO; (b) AFM image of GO; (c) FT-IR spectra of graphite and GO; (d) XPS wide-scan spectra of GO; (e) C1s core level spectrum of GO.

GO dispersion, GE solution, and GE/GO complex dispersion at pH of 4.0. Due to the strong interactions between GE and GO under the specific condition, GE/GO complex forms and precipitates in water upon mixing of GO dispersion and GE solution.

3.2. Characterization of membrane

3.2.1. Surface morphology and thickness of hybrid multilayer membranes

The surface morphologies of different membranes were characterized by FESEM. There exist abundant nanopores on PAN membrane surface with homogeneous distribution (Fig. 3a). After hydrolyzation treatment, pore shrinkage occurs with obvious reduction of nanopore size (Fig. 3b). After the first deposition of GE solution on H-PAN (i.e. $(GE/GO)_{0.5}$/H-PAN membrane), the nanopores still exist and are not covered by GE (Fig. 3c) due to the infiltration of low-concentration GE solution into nanopores [1]. In conventional LbL self-assembly process of polyelectrolytes, a large number of bilayers are required to fully cover the nanopores on substrate and then form a defect-free layer [19,26]. In this study, the subsequent deposition of GO can solve this problem. As shown in Fig. 3d, no nanopores exist on $(GE/GO)_1$/H-PAN membrane surface, due to the micrometer-scale size of GO along horizontal direction, as well as the even spreading and packing

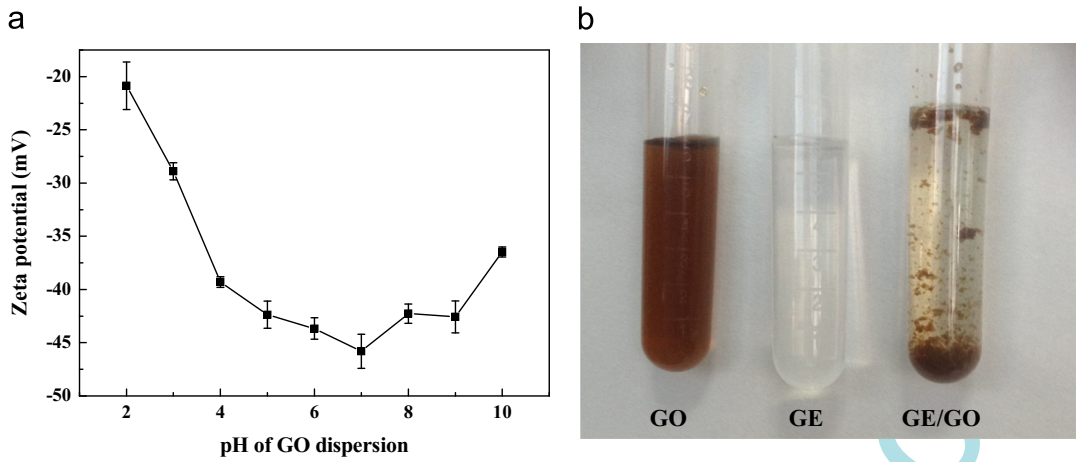

Fig. 2. (a) Zeta potential of GO dispersion at different pH values; (b) images of GO dispersion, GE solution, and GE/GO complex dispersion at pH of 4.0.

of GO on membrane surface resulting from the appropriate pH condition [22]. As a result, the required deposition cycle number for fabricating defect-free layer is reduced, thus greatly simplifying the membrane fabrication procedure. Compared Fig. 3e and f, it can be observed that GE/H-PAN possesses a smooth surface, while some wrinkles resulted from GO appear on the surface of $(GE/GO)_{10.5}$/H-PAN membrane.

The cross-section morphologies of GE/H-PAN and $(GE/GO)_{10.5}$/H-PAN membranes were characterized by FESEM as shown in Fig. 4. Compared with GE/H-PAN membrane, $(GE/GO)_{10.5}$/H-PAN membrane exhibits a more pronounced boundary between the active layer and the support layer, which can be ascribed to the presence of GO: For GE/H-PAN membrane, GE solution infiltrates into and fills up the nanopores on support layer, which results in an indistinct boundary [19]; in the case of $(GE/GO)_{10.5}$/H-PAN membrane, the coverage of GO for nanopores on support layer (as shown in Fig. 3d) inhibits the infiltration of GE solution. As a result, a distinct boundary between GE/GO active layer and H-PAN support layer is formed. The thicknesses of active layers in both membranes were obtained from the cross-section images, on which at least ten different locations were measured and averaged to acquire the final result. The thickness of $(GE/GO)_{10.5}$/H-PAN membrane is only 115 ± 10 nm (Fig. 4b), lower than those of most current separation membranes. Additionally, the thickness of GE/H-PAN membrane is 108 ± 12 nm, close to that of $(GE/GO)_{10.5}$/H-PAN membrane.

3.2.2. *Chemical structure and hydrophilicity of hybrid multilayer membranes*

Fig. 5 depicts the FT-IR spectra of PAN, H-PAN and $(GE/GO)_{10.5}$/H-PAN membranes. Compared the spectra of PAN and H-PAN membranes, it is observed that the characteristic peak of cyano group at 2243 cm^{-1} weakens, and new peaks at 3360 cm^{-1} (stretching vibration of hydroxyl), 1657 cm^{-1} (stretching vibration of carbonyl in carboxyl), and 1569 cm^{-1} (asymmetrical stretching vibration of carboxylate) appear after hydrolyzation treatment, verifying the conversion of a portion of cyano groups on PAN into carboxyl and carboxylate groups. The characteristic peak of cyano group further weakens after alternate deposition of GE and GO due to the coverage of H-PAN membrane. Moreover, a strong peak at 1657 cm^{-1} appears on the spectrum of $(GE/GO)_{10.5}$/H-PAN membrane, which can be ascribed to the stretching vibration of carbonyl in abundant amide groups of GE. The peak at 3360 cm^{-1} strengthens and shifts towards the lower wave number region, resulting from the enormous hydroxyl, carboxyl, and amino groups on GE and GO, and the hydrogen bonds between these polar groups.

The hydrophilicity of different membrane surfaces was evaluated by measuring the static water contact angles. It is shown in Fig. 6 that PAN membrane exhibits a remarkable increase of hydrophilicity after hydrolyzation treatment with contact angle decreasing from 63.6° (PAN membrane) to 29.3° (H-PAN membrane). This can be ascribed to the conversion of abundant cyano groups on PAN to carboxylate and carboxyl groups. Compared with GE/H-PAN pristine membrane (62.6°), the outermost GE layer of hybrid multilayer membranes possesses slightly lower contact angles, which results from the abundant wrinkles on membrane surface (as shown in Fig. 3f). The alternate variation of contact angles confirms the successful LbL self-assembly process of GE and GO.

3.2.3. *Thermal property analysis*

TGA curves of GE membrane and GE/GO complex were obtained to investigate the variation of GE thermal property after interacting with GO [18]. GE/GO complex was prepared through filtrating and drying the precipitation formed upon mixing of GO dispersion and GE solution. As shown in Fig. 7, GE membrane possesses two weight loss stages (evaporation of water, and decomposition of GE molecules), while GE/GO complex possesses three weight loss stages (evaporation of water, pyrolysis of the oxygen-containing functional groups on GO, and decomposition of GE molecules). The GE/GO complex starts to lose weight at an earlier time than GE membrane (about 150 °C) after water evaporation stage, seemingly indicating the lower thermal stability of GE/GO complex than GE membrane. However, the weight loss is because of the pyrolysis of the oxygen-containing functional groups on GO [13], and not relevant to GE molecules. The thermal degradation behaviors of GE molecules in GE membrane and GE/GO complex (i.e. the second stage on blue curve and the third stage on red curve) are compared to evaluate the thermal properties of GE molecules. It is shown that the initial degradation temperature for GE membrane is 289.5 °C, while it increases to 310.7 °C for GE molecules in GE/GO complex. The remarkably enhanced initial degradation temperature implies the improved thermal stability of GE molecules after combining with GO. Therefore, it can be concluded that the thermal stability of GE molecules in as-fabricated hybrid multilayer membranes was enhanced compared with that in GE/H-PAN pristine membrane. The improved thermal stability of GE molecules arises from the existence of interactions between GE and GO, which inhibits the mobility of GE molecular chains. After the pyrolysis of oxygen-containing groups in the temperature range of 150 °C–250 °C, GO is merely left with hydrophobic carbon backbone, which can only form hydrophobic interactions with GE. Therefore, the

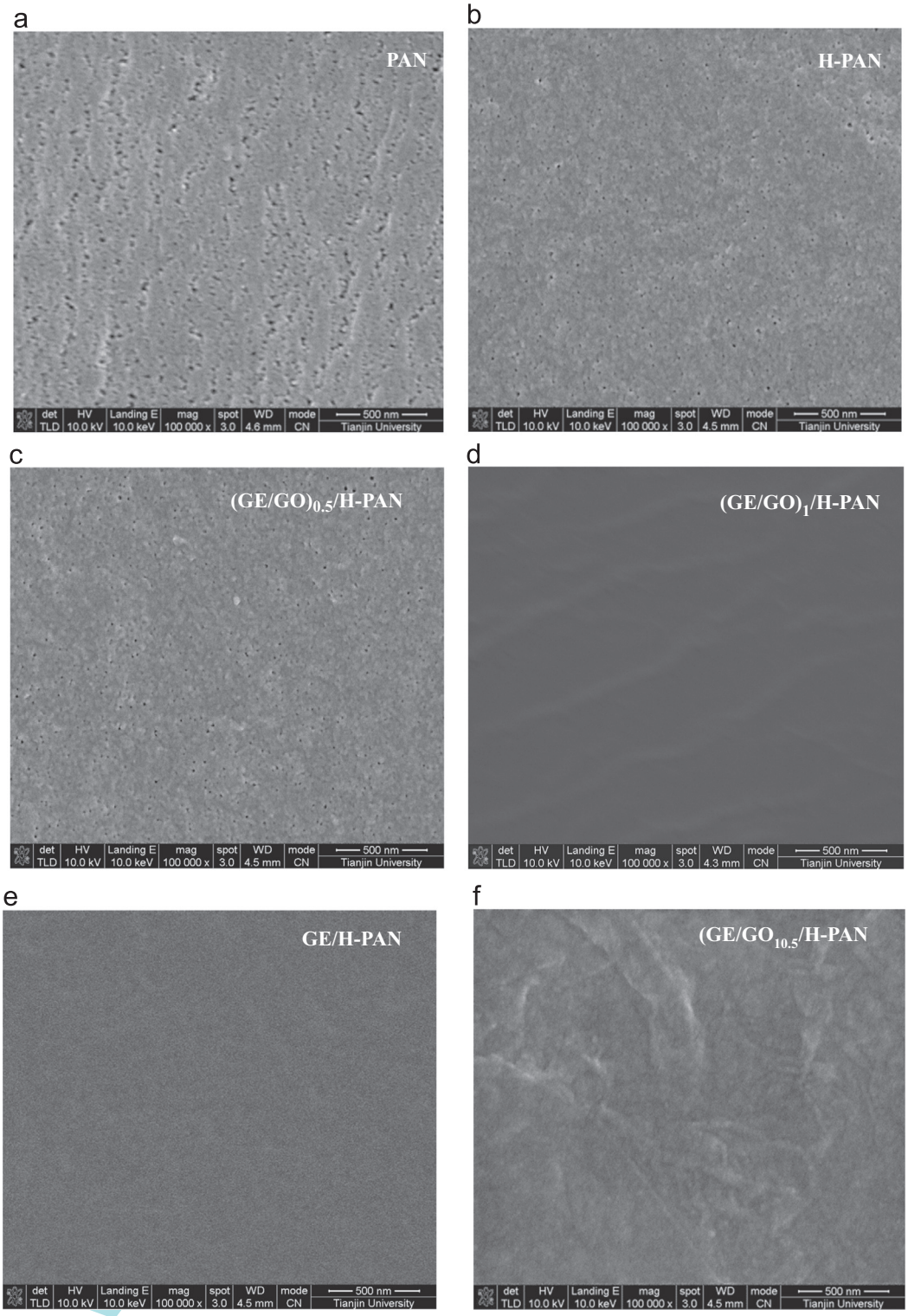

Fig. 3. FESEM images of membrane surface morphologies: (a) PAN membrane; (b) H-PAN membrane; (c) $(GE/GO)_{0.5}$/H-PAN membrane; (d) $(GE/GO)_1$/H-PAN membrane; (e) GE/H-PAN membrane; (f) $(GE/GO)_{10.5}$/H-PAN membrane.

enhancement of initial degradation temperature verifies the formation of hydrophobic interactions between GE and GO.

3.2.4. *Analysis of multiple interactions in hybrid multilayer membrane*

According to the above results, the multiple interactions between GE, GO, and H-PAN in the hybrid multilayer membrane are analyzed and shown in Fig. 8. After alkali hydrolyzing treatment, carboxylate and carboxyl groups are generated on the surface of PAN substrate, which can form electrostatic attraction and hydrogen bond with GE, thus achieving the deposition of first layer on substrate. The subsequent deposition of GE and GO involves various types of interactions: the ionized carboxyl groups on GO can form electrostatic attractions with the protonated amino groups on GE; the various polar groups on GE (such as

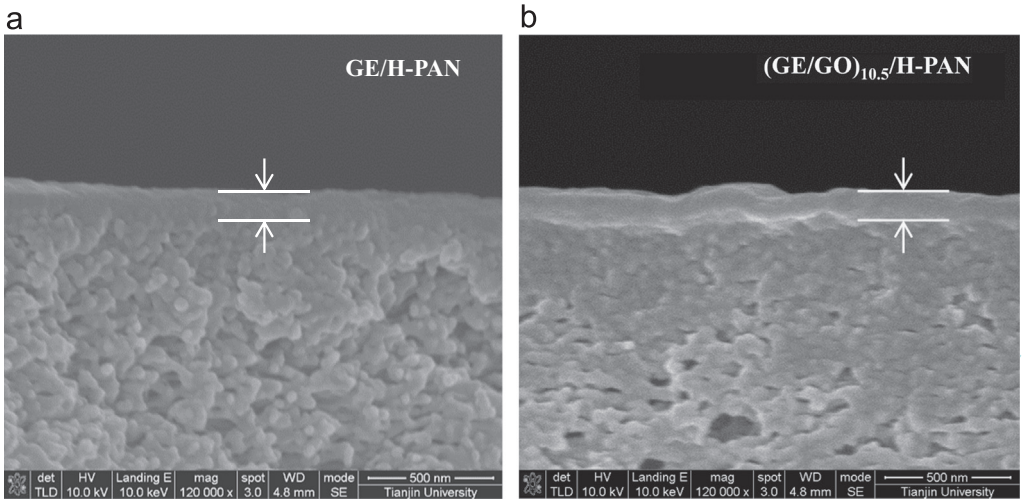

Fig. 4. FESEM images of membrane cross-section morphologies: (a) GE/H-PAN membrane; (b) $(GE/GO)_{10.5}$/H-PAN membrane.

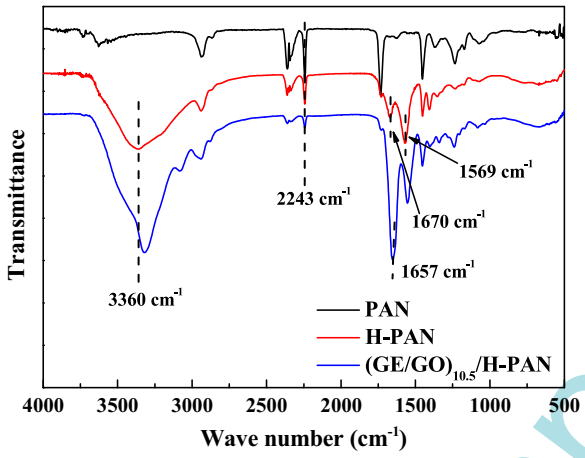

Fig. 5. FT-IR spectra of PAN, H-PAN and $(GE/GO)_{10.5}$/H-PAN membranes.

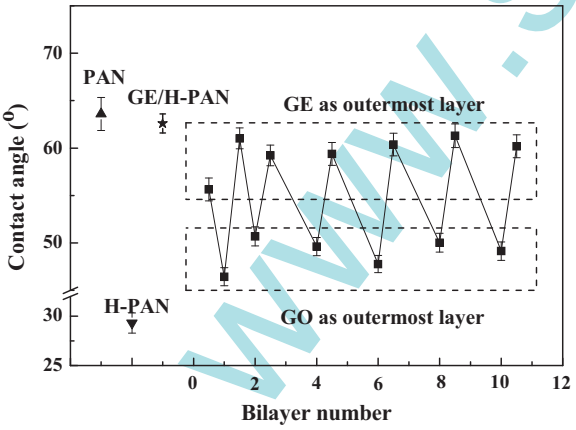

Fig. 6. Water contact angles on different membrane surfaces.

amino, carboxyl, and carbonyl groups) and GO (such as hydroxyl, epoxy, and carboxyl groups) can form hydrogen bonds; the carbon backbone of GO can form hydrophobic interactions with the hydrophobic amino acid side chains on GE (such as aromatic ring and pyrrolidine ring). The combination of electrostatic attraction, hydrogen bond and hydrophobic interaction ensures the efficient LbL self-assembly process of GE and GO.

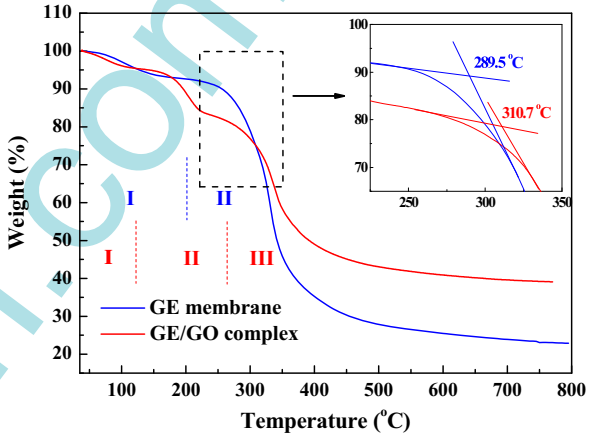

Fig. 7. TGA curves of GE membrane and GE/GO complex. (For interpretation of the references to color in this figure legend, the reader is referred to the web version of this article.)

3.3. Pervaporation experiment

3.3.1. Effect of bilayer number and pH value

In order to investigate the impacts of GO incorporation and bilayer number on membrane separation performance, pervaporation experiments of GE/H-PAN pristine membrane and hybrid multilayer membranes were conducted with 90 wt% ethanol aqueous solution at 350 K (Fig. 9). Compared with GE/H-PAN membrane, the $(GE/GO)_{10.5}$/H-PAN membrane exhibits superior pervaporation performance with the permeation flux, separation factor and PSI value increasing to 1.26, 2.16, 2.74-fold, respectively. Due to the similar thicknesses of these two membranes, the discrepancy in their pervaporation performance can be primarily ascribed to the incorporation of GO. First, the diffusion pathways become more tortuous after incorporating GO [16], thus increasing the diffusion resistance for water/ethanol molecules. Second, the multiple interactions between GE and GO disturb the ordered arrangement of GE molecules, thus decreasing GE crystallinity [5,9,27] and increasing the diffusion rates of water and ethanol molecules in polymeric region. Third, the oxygen-containing groups on GO edges and defects exhibit high water-affinity and provide transport pathways favorable for water molecules. Last, pore-filling of H-PAN support layer by GE solution is obviously inhibited by GO (as shown in Fig. 4), which achieves a lower effective thickness of active layer than GE/H-PAN membrane

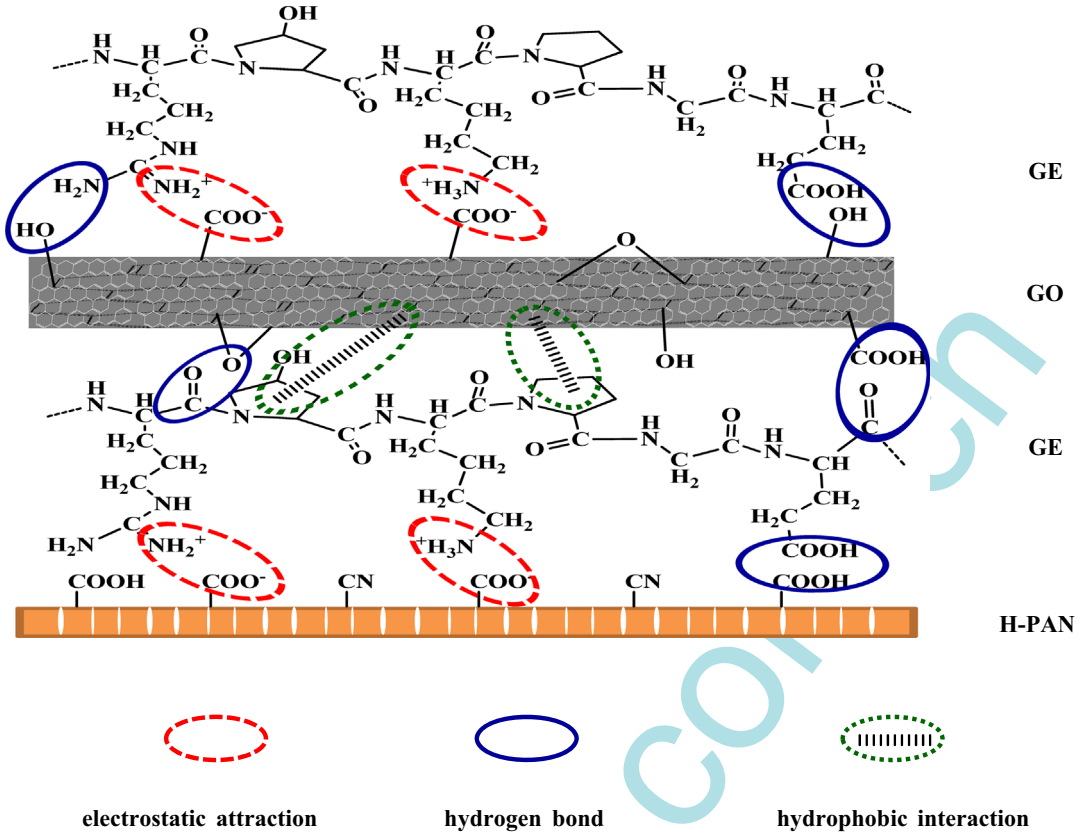

Fig. 8. Schematic representation of the interfacial interactions in hybrid multilayer membrane.

[28,29]. The combination of above factors leads to increased water flux, decreased ethanol flux, as well as the resultant higher separation factor and PSI value. In addition, it is observed that the separation factor and PSI value increase, while the permeation flux decrease continuously with the bilayer number of hybrid multilayer membranes varying from 2.5 to 10.5. The variation of pervaporation performance can be ascribed to the following two reasons: the increased membrane thickness and elongated diffusion pathway with bilayer number increase the diffusion resistance for water/ethanol molecules; the non-selective defects exist in less-bilayer membranes are gradually covered with continuous deposition of GE and GO [22], thus forming defect-free active layer and increasing diffusion resistance. For membranes with low bilayer numbers, both reasons play vital roles, leading to rapid decrease of permeation flux (with bilayer number increasing from 2.5 to 4.5). With the increase of bilayer number, the contribution of latter reason lessens due to the gradually disappeared defects, thus resulting in slow decrease of permeation flux (with bilayer number increasing from 4.5 to 10.5). It can be observed from Fig. 9b that ethanol flux decreases more obviously than water flux, which is attributed to the larger size of ethanol molecule and the sequent more significantly increased diffusion resistance. With the bilayer number increasing from 2.5 to 10.5, water flux decreases by 34.5%, while ethanol flux exhibits a decrease of 86.8%. Consequently, the separation factor achieves drastic enhancement, resulting in the sharp increase of PSI value.

The effect of pH value during self-assembly process on membrane separation performance was investigated as listed in Table 1. When the pH value of GE solution and GO dispersion is 2.0, the lower charge density on GO leads to aggregation [22], which results in the uneven spreading and packing of GO and decreases the interaction sites between GE and GO. Furthermore, the subsequent deposition of GE is also influenced with uneven deposition and decreased deposition amount. As a result, defects may exist in the as-fabricated membranes which lead to higher permeation flux and lower separation factor. When the pH value is 6.0, GO possesses higher charge density and the resultant desirable dispersity. Nevertheless, the decreasing amount of protonated amino groups on GE compared with that under pH of 4.0 reduces the interaction site of electrostatic attraction between GE and GO, and then weakens the interfacial interaction. Consequently, the decreased deposition amount and loose membrane structure are generated, leading to higher permeation flux and lower separation factor [19,23]. In summary, the pH value of 4.0 was determined as the optimal condition of self-assembly process in terms of separation performance.

3.3.2. *Effect of operation temperature*

The pervaporation experiments of $(GE/GO)_{10.5}$/H-PAN membrane under different temperatures ranging from 313 to 350 K were performed with 90 wt% ethanol aqueous solution. It is shown in Fig. 10 that the membrane achieves simultaneous increase of permeation flux and separation factor with the increase of operation temperature. In order to analyze the effects of operation temperature on water/ethanol permeation, water/ethanol permeance (driving force-normalized form of permeation flux) and selectivity were calculated and shown in Table 2. With the increase of temperature, water permeance keeps increasing, while ethanol permeance exhibits a reverse tendency. It can be deduced that positive factors for water permeation are dominant including the loosened membrane structure and the weakened coupling effect between water and ethanol with temperature increasing, which eventually increase water permeance. By contrast, negative factors contribute more to ethanol permeation: higher temperature suppresses the adsorption of ethanol on membrane surface

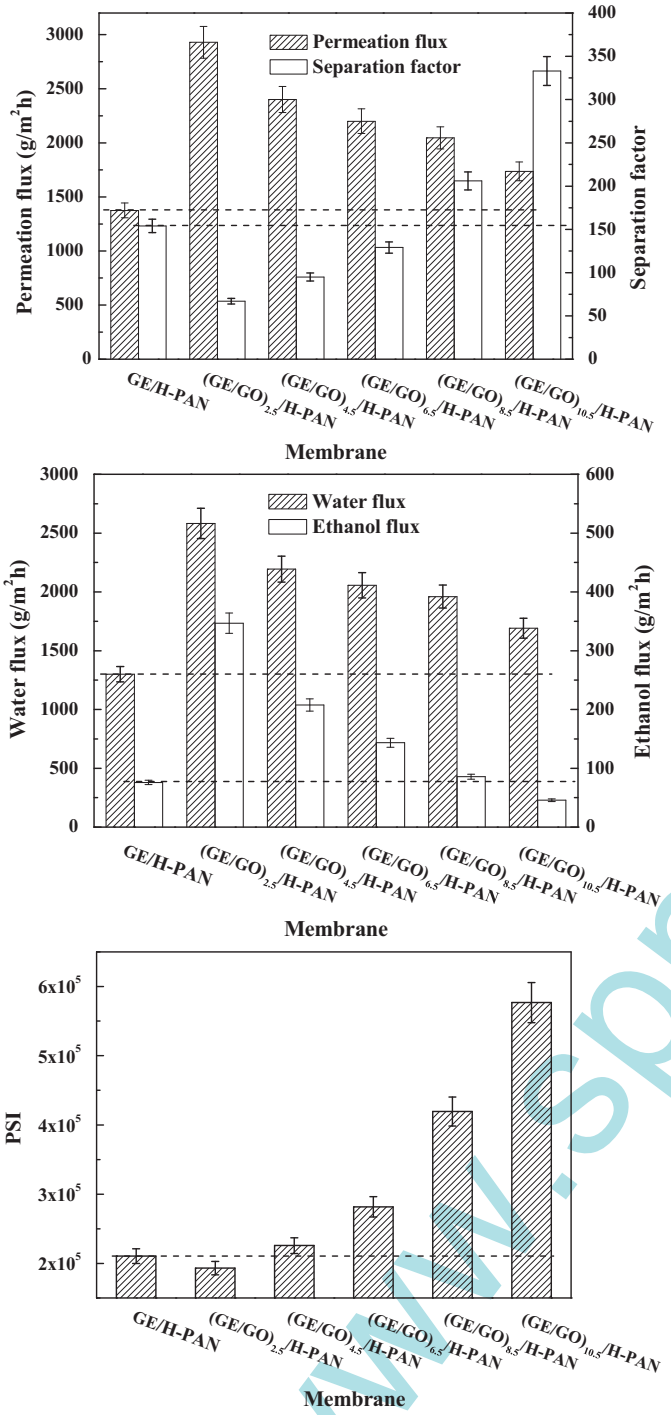

Fig. 9. Pervaporation performance of GE/H-PAN pristine membrane and hybrid multilayer membranes with different bilayer number: (a) permeation flux and separation factor; (b) water flux and ethanol flux; (c) PSI value.

Table 1
Pervaporation performance of hybrid multilayer membranes fabricated under different pH values.

pH value	Permeation flux (g/m² h)	Separation factor	Water content in permeate (wt%)	PSI (10^5)
2.0	2821	65	87.8	1.81
4.0	1737	333	97.4	5.77
6.0	2215	157	94.6	3.46

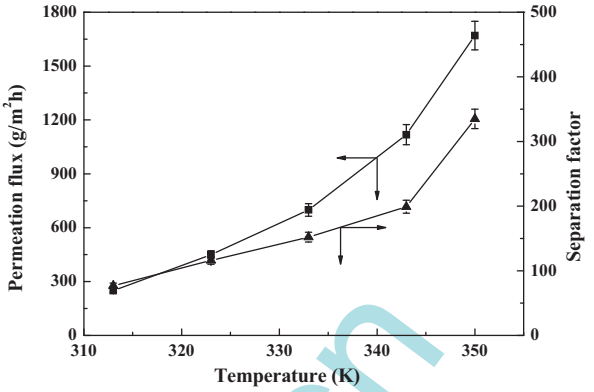

Fig. 10. Effect of temperature on the pervaporation performance of $(GE/GO)_{10.5}$/H-PAN membrane.

Table 2
Water/ethanol permeance and selectivity of $(GE/GO)_{10.5}$/H-PAN membrane under different temperatures.

Temperature (K)	$(P/l)_W$ (GPU)	$(P/l)_E$ (GPU)	Selectivity
313	3142	32	97
323	3523	25	141
333	3444	19	182
343	3512	15	235
350	4342	10	418

[23], the weakened coupling effect between water and ethanol inhibits the diffusion of ethanol along with water molecules [30], thus decreasing ethanol permeance. As a result, the selectivity is continuously enhanced with operation temperature, indicating that appropriately high operation temperature is desirable for preferential permeation of water over ethanol.

3.3.3. *Effect of water content in feed*

The effect of water content in feed on the pervaporation performance of $(GE/GO)_{10.5}$/H-PAN membrane was investigated at 350 K. It is shown in Fig. 11a that both permeation flux and water content in permeate increase with the water content in feed increasing from 5 wt% to 20 wt%. A desirable pervaporation performance is obtained with the permeation flux of 2275 g/m² h and water content in permeate of 98.7 wt% when the water content in feed is 20 wt%. In order to analyze the effects of water content in feed on pervaporation performance, water/ethanol permeance and selectivity were calculated and shown in Fig. 11b. The water permeance increases remarkably at first and then fluctuates inappreciably, while the ethanol permeance continues to increase. Consequently, the selectivity increases at the beginning and then decreases with the maximum value obtained at water content in feed of 10 wt%. The variation of water/ethanol permeance and selectivity with water content in feed is ascribed to the joint plasticization effect and coupling effect [31–33]. In the range of 5 wt% to 10 wt%, the plasticization effect of water on membrane dominates, which causes membrane swelling, loosened membrane structure, resulting in significant increase of water/ethanol permeance. After that, the coupling effect between water and ethanol becomes serious and contributes more [34,35]. Increasing ethanol molecules interact and form clusters with water molecules, which inhibits the adsorption and diffusion of water (fast component) in membrane by blocking the interaction between water and membrane material and increasing diffusion resistance of water molecules, respectively [30]. For ethanol molecules (slow component), the coupling effect generates

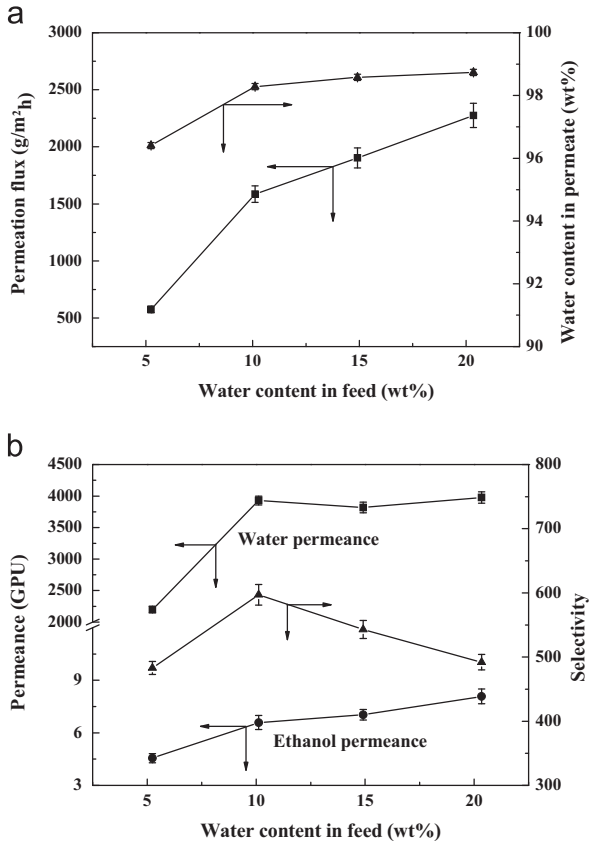

Fig. 11. Effect of water content in feed on the pervaporation performance of $(GE/GO)_{10.5}$/H-PAN membrane: (a) permeation flux and water content in permeate; (b) water/ethanol permeance and selectivity.

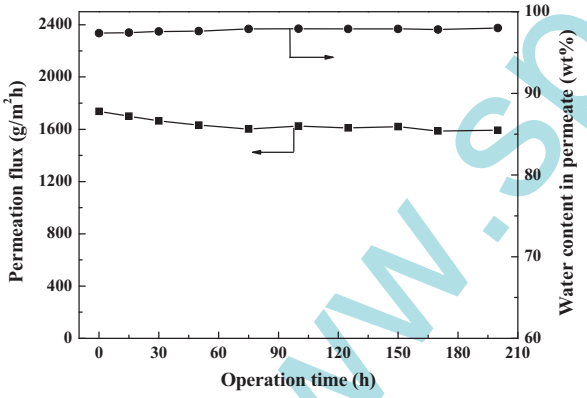

Fig. 12. Long-term pervaporation performance of $(GE/GO)_{10.5}$/H-PAN membrane.

positive impacts: both adsorption and diffusion of ethanol can be enhanced due to the formation of water/ethanol clusters [30]. The continuously increased permeation flux and water content in permeate within the given range indicate that appropriately high water content in feed is desirable for achieving high separation capacity and efficiency.

3.3.4. Long-term operation stability

In practical application, long-term operation stability is a vital index to evaluate membrane performance. Fig. 12 shows the pervaporation performance of $(GE/GO)_{10.5}$/H-PAN membrane up to 200 h for 90 wt% ethanol aqueous solution at 350 K. The permeation flux slightly decreases and stabilizes at about 1600 g/(m^2 h) after 75 h, while the water content in permeate increases at first and then stabilizes at about 98.0 wt%. The desirable operation stability indicates the structural stability of as-prepared hybrid multilayer membrane and its great application potential.

3.3.5. Comparison of pervaporation performance of GO-based membranes

Fig. S5 exhibits some pervaporation performance data of GO-based membranes (GO membranes and polymer/GO hybrid membranes fabricated via LbL self-assembly) for ethanol dehydration in literatures and this study. It can be observed that the membranes in this study exhibit comparable performance, and especially relatively higher permeation flux (Fig. S5a), which is an essential index for the industrial application of membrane. Considering the different operation conditions in literatures, water permeance and selectivity were also calculated and shown in Fig. S5b. Both the water permeance and selectivity of membranes in this study are acceptable compared with literature data.

4. Conclusion

Ultrathin hybrid membranes were fabricated through LbL self-assembly of GE and GO on H-PAN membranes driven by multiple interactions and utilized for water/ethanol separation. Electrostatic attractions were formed between ionized carboxyl groups on GO and protonated amino groups on GE, hydrogen bonds were formed between various polar groups on GE and GO, hydrophobic interactions were formed between hydrophobic carbon backbone of GO and hydrophobic amino acid side chains on GE. The alternate variation of water contact angles demonstrated the successful assembly. In membrane fabrication process, the deposition of GO could cover the nanopores on H-PAN membrane due to the micrometer-scale size of GO along horizontal direction, as well as the homogeneous spreading and packing of GO on membrane surface. Consequently, the required deposition cycles for acceptable permselectivity of membrane was reduced compared with conventional LbL self-assembly process of polyelectrolytes, thus simplifying the membrane-fabrication procedure and obtaining ultrathin membranes with thicknesses lower than 115 nm. The optimum pH value for self-assembly process was determined as 4.0 in order to obtain high separation performance. Compared with GE/H-PAN pristine membrane, incorporation of GO led to more tortuous diffusion pathway, abundant hydrophilic groups on GO, decreased GE crystallinity, and inhibited pore infiltration. The above factors influenced water/ethanol permeation synergistically and rendered the hybrid multilayer membranes improved separation performance with permeation flux, separation factor and PSI value increasing to 1.26, 2.16, 2.74-fold synchronously. Desirable long-term operation stability of the hybrid multilayer membrane was also demonstrated.

Acknowledgments

The authors gratefully acknowledge the financial support from the National Science Fund for Distinguished Young Scholars (No. 21125627), the National Natural Science Foundation of China (Nos. 21490583 and 21306131), Specialized Research Fund for the Doctoral Program of Higher Education (20120032120009), Seed Foundation of Tianjin University (NO. 2014XJJ-0019), and the Program of Introducing Talents of Discipline to Universities (No. B06006).

Appendix A. Supporting information

Supplementary data associated with this article can be found in the online version at http://dx.doi.org/10.1016/j.memsci.2015.03.073.

Nomenclature

Variables

A	membrane area (m^2)
A_i	pre-exponential factor of component i
E_i	apparent activation energy of component i (kJ/mol)
F_E	mass fraction of ethanol in feed solution (wt%)
F_W	mass fraction of water in feed solution (wt%)
J	permeation flux (g/m^2 h)
J_i	permeation flux of component i (g/m^2 h)
l	membrane thickness (m)
P_E	mass fraction of ethanol in permeate solution (wt%)
P_W	mass fraction of water in permeate solution (wt%)
$(P/l)_E$	ethanol permeance (GPU)
$(P/l)_W$	water permeance (GPU)
p_{i0}	partial pressures of component i in the feed side (Pa)
p_{il}	partial pressures of component i in the permeate side (Pa)
p_{i0}^{sat}	saturated vapor pressure of pure component i at operation temperature (Pa)
Q	mass of permeate (g)
R	gas constant
T	operation temperature (K)
t	time interval (h)
X	bilayer number of hybrid multilayer membranes
x_{i0}	mole fraction of component i

Greek letters

α	separation factor
β	selectivity
γ_{i0}	activity coefficient of component i
θ	diffraction angle (deg)

Abbreviations

PSI	pervaporation separation index

References

[1] N. Joseph, P. Ahmadiannamini, R. Hoogenboom, I.F.J. Vankelecom, Layer-by-layer preparation of polyelectrolyte multilayer membranes for separation, Polym. Chem. 5 (2014) 1817–1831.

[2] M.I. Lopez, P.E. Meza Martinez, M.A. Meyers, Organic interlamellar layers, mesolayers and mineral nanobridges: contribution to strength in abalone (Haliotis rufescence) nacre, Acta Biomater. 10 (2014) 2056–2064.

[3] Z. Tang, N.A. Kotov, S. Magonov, B. Ozturk, Nanostructured artificial nacre, Nat. Mater. 2 (2003) 413–418.

[4] J.F. Wang, Q.F. Cheng, L. Lin, L. Jiang, Synergistic toughening of bioinspired poly (vinyl alcohol)-clay-nanofibrillar cellulose artificial nacre, ACS Nano 8 (2014) 2739–2745.

[5] J. Zhu, H.N. Zhang, N.A. Kotov, Thermodynamic and structural insights into nanocomposites engineering by comparing two materials assembly techniques for graphene, ACS Nano 7 (2013) 4818–4829.

[6] I.A. Aksay, M. Trau, S. Manne, I. Honma, N. Yao, L. Zhou, P. Fenter, P. M. Eisenberger, S.M. Gruner, Biomimetic pathways for assembling inorganic thin films, Science 273 (1996) 892–898.

[7] H.B. Yao, H.Y. Fang, Z.H. Tan, L.H. Wu, S.H. Yu, Biologically inspired, strong, transparent, and functional layered organic-inorganic hybrid films, Angew. Chem. 49 (2010) 2140–2145.

[8] K. Hu, M.K. Gupta, D.D. Kulkarni, V.V. Tsukruk, Ultra-robust graphene oxide-silk fibroin nanocomposite membranes, Adv. Mater. 25 (2013) 2301–2307.

[9] Y.Q. Li, T. Yu, T.Y. Yang, L.X. Zheng, K. Liao, Bio-inspired nacre-like composite films based on graphene with superior mechanical, electrical, and biocompatible properties, Adv. Mater. 24 (2012) 3426–3431.

[10] X. Zhao, Q. Zhang, Y. Hao, Y. Li, Y. Fang, D. Chen, Alternate multilayer films of poly(vinyl alcohol) and exfoliated graphene oxide fabricated via a facial layer-by-layer assembly, Macromolecules 43 (2010) 9411–9416.

[11] R.R. Nair, H.A. Wu, P.N. Jayaram, I.V. Grigorieva, A.K. Geim, Unimpeded permeation of water through helium-leak-tight graphene-based membranes, Science 335 (2012) 442–444.

[12] T.M. Yeh, Z. Wang, D. Mahajan, B.S. Hsiao, B. Chu, High flux ethanol dehydration using nanofibrous membranes containing graphene oxide barrier layers, J. Mater. Chem. A 1 (2013) 12998–13003.

[13] Y.P. Tang, D.R. Paul, T.S. Chung, Free-standing graphene oxide thin films assembled by a pressurized ultrafiltration method for dehydration of ethanol, J. Membr. Sci. 458 (2014) 199–208.

[14] Y. Shi, S. Jiang, K. Zhou, C. Bao, B. Yu, X. Qian, B. Wang, N. Hong, P. Wen, Z. Gui, Y. Hu, R.K. Yuen, Influence of g-C3N4 nanosheets on thermal stability and mechanical properties of biopolymer electrolyte nanocomposite films: a novel investigation, ACS Appl. Mater. Interfaces 6 (2014) 429–437.

[15] A.A. Vasileiou, M. Kontopoulou, A. Docoslis, A noncovalent compatibilization approach to improve the filler dispersion and properties of polyethylene/graphene composites, ACS Appl. Mater. Interfaces 6 (2014) 1916–1925.

[16] Y.H. Yang, L. Bolling, M.A. Priolo, J.C. Grunlan, Super gas barrier and selectivity of graphene oxide-polymer multilayer thin films, Adv. Mater. 25 (2013) 503–508.

[17] M. Hu, B. Mi, Layer-by-layer assembly of graphene oxide membranes via electrostatic interaction, J. Membr. Sci. 469 (2014) 80–87.

[18] N. Wang, S. Ji, G. Zhang, J. Li, L. Wang, Self-assembly of graphene oxide and polyelectrolyte complex nanohybrid membranes for nanofiltration and pervaporation, Chem. Eng. J. 213 (2012) 318–329.

[19] J. Zhao, F. Pan, P. Li, C. Zhao, Z. Jiang, P. Zhang, X. Cao, Fabrication of ultrathin membrane via layer-by-layer self-assembly driven by hydrophobic interaction towards high separation performance, ACS Appl. Mater. Interfaces 5 (2013) 13275–13283.

[20] F. Pan, Q. Cheng, H. Jia, Z. Jiang, Facile approach to polymer-inorganic nanocomposite membrane through a biomineralization-inspired process, J. Membr. Sci. 357 (2010) 171–177.

[21] W.S. Hummers Jr., R.E. Offeman, Preparation of graphitic oxide, J. Am. Chem. Soc. 80 (1958) 1339.

[22] J.T. Chen, Y.J. Fu, Q.F. An, S.C. Lo, S.H. Huang, W.S. Hung, C.C. Hu, K.R. Lee, J. Y. Lai, Tuning nanostructure of graphene oxide/polyelectrolyte LbL assemblies by controlling pH of GO suspension to fabricate transparent and super gas barrier films, Nanoscale 5 (2013) 9081–9088.

[23] K. Cao, Z. Jiang, J. Zhao, C. Zhao, C. Gao, F. Pan, B. Wang, X. Cao, J. Yang, Enhanced water permeation through sodium alginate membranes by incorporating graphene oxides, J. Membr. Sci. 469 (2014) 272–283.

[24] L. Ye, J. Fu, Z. Xu, R. Yuan, Z. Li, Facile one-pot solvothermal method to synthesize sheet-on-sheet reduced graphene oxide (RGO)/$ZnIn_2S_4$ nanocomposites with superior photocatalytic performance, ACS Appl. Mater. Interfaces 6 (2014) 3483–3490.

[25] W. Zhang, S. Wang, J. Ji, Y. Li, G. Zhang, F. Zhang, X. Fan, Primary and tertiary amines bifunctional graphene oxide for cooperative catalysis, Nanoscale 5 (2013) 6030–6033.

[26] L. Krasemann, A. Toutianoush, B. Tieke, Self-assembled polyelectrolyte multilayer membranes with highly improved pervaporation separation of ethanol/water mixtures, J. Membr. Sci. 181 (2001) 221–228.

[27] D.P. Suhas, A.V. Raghu, H.M. Jeong, T.M. Aminabhavi, Graphene-loaded sodium alginate nanocomposite membranes with enhanced isopropanol dehydration performance via a pervaporation technique, RSC Adv. 3 (2013) 17120–17130.

[28] F. Hamad, K. Khulbe, T. Matsuura, Comparison of gas separation performance and morphology of homogeneous and composite PPO membranes, J. Membr. Sci. 256 (2005) 29–37.

[29] E. Shi, W. Huang, Z. Xiao, D. Li, M. Tang, Influence of binding interface between active and support layers in composite PDMS membranes on permeation performance, J. Appl. Polym. Sci. 104 (2007) 2468–2477.

[30] R. Jiraratananon, A. Chanachai, R.Y.M. Huang, Pervaporation dehydration of ethanol–water mixtures with chitosan/hydroxyethylcellulose (CS/HEC) composite membranes: II. Analysis of mass transport, J. Membr. Sci. 199 (2002) 211–222.

[31] J. Ren, C. Jiang, The coupling effect of the thermodynamic swelling process in pervaporation, J. Membr. Sci. 140 (1998) 221–233.

[32] V.T. Magalad, G.S. Gokavi, C. Ranganathaiah, M.H. Burshe, C. Han, D. D. Dionysiou, M.N. Nadagouda, T.M. Aminabhavi, Polymeric blend nanocomposite membranes for ethanol dehydration—effect of morphology and membrane–solvent interactions, J. Membr. Sci. 430 (2013) 321–329.

[33] S.G. Adoor, L.S. Manjeshwar, S.D. Bhat, T.M. Aminabhavi, Aluminum-rich zeolite beta incorporated sodium alginate mixed matrix membranes for pervaporation dehydration and esterification of ethanol and acetic acid, J. Membr. Sci. 318 (2008) 233–246.

[34] F. Lipnizki, S. Hausmanns, Hydrophobic pervaporation of binary and ternary solutions: evaluation of fluxes, selectivities, and coupling effects, Sep. Sci. Technol. 39 (2005) 2235–2259.

[35] R. Guo, C. Hu, B. Li, Z. Jiang, Pervaporation separation of ethylene glycol/water mixtures through surface crosslinked PVA membranes: coupling effect and separation performance analysis, J. Membr. Sci. 289 (2007) 191–198.